Hindawi
Mathematical Problems in Engineering
Volume 2022, Article ID 5576194, 11 pages
https://doi.org/10.1155/2022/5576194

Research Article

Analytical Simulation of Heat and Mass Transmission in Casson Fluid Flow across a Stretching Surface

Kashif Ali Khan,[1] Faizan Jamil,[1] Javaid Ali,[2] Ilyas Khan,[3] Nauman Ahmed,[4] Mulugeta Andualem,[5] and Muhammad Rafiq[6]

[1]*Department of Mathematics, University of Engineering and Technology, Lahore, Pakistan*
[2]*Department of Mathematics, GCT, Punjab Higher Education Department, Lahore, Pakistan*
[3]*Department of Mathematics, College of Science Al-Zulfi, Majmaah University, Al-Majmaah 11952, Saudi Arabia*
[4]*Department of Mathematics and Statistics, The University of Lahore, Lahore, Pakistan*
[5]*Department of Mathematics, Bonga University, Bonga, Ethiopia*
[6]*Department of Mathematics, Faculty of Sciences, University of Central Punjab, Lahore, Pakistan*

Correspondence should be addressed to Mulugeta Andualem; mulugetaandualem4@gmail.com

Received 16 January 2021; Revised 30 November 2021; Accepted 24 January 2022; Published 15 February 2022

Academic Editor: Amin Jajarmi

This research presents a review of an analytical simulation of heat and mass transmission features of steady, non-Newtonian Casson fluid motion across a permeable medium through a stretching surface. The effects of heat production and thermal emission are put into discussion. Mathematically, the governing model is manipulated by a series of nonlinear partial equations, which are then modified into ordinary differential equations with the assistance of appropriate conversion. Analytical results for such equations are then achieved by invoking the notable technique of the homotopy analysis method (HAM), and its solution sounds good while achieving the convergence guaranteed in the convergence table. Some achievements have been made. The consequence of raising the value of the Casson parameter is comprehended to be putting down the velocity field while increasing the temperature field. Also, the concentration field falls with an increase in the Schmidt number, while it rises with an enhancement in the Soret number. The electric parameter due to Lorentz's force is capable of accelerating the temperature of the fluid but downsizing the velocity.

1. Introduction

In advanced technology, several flow properties are not understood with the Newtonian flow model. As a result, the non-Newtonian fluid concept is becoming more beneficial. Some of the significant and recent studies [1–5] about it are useful for the readers. The research scientist has gained attention for Casson fluids because of their impressive technical and industrial science characteristics. Casson fluid is among the significant types of fluid in the class of non-Newtonian substances. It is a shear-diminishing substance that is expected to have a zero-shear rate of infinite viscosity, i.e., beyond yield stress, no flow keeps going and viscosity tends to be zero at a shear rate of infinity. Common examples of Casson fluids are synthetic lubricants, sugar solutions, mud drilling, coating of clay, certain oil paints, and biological fluids. Widely available Casson fluid models are categorized as conscious rheological properties such as Oldroyd-B, Eyring-Powell, Seely, Cumbersome, Oldroyd-A, Casson, Maxwell, Carreau, Jeffrey, and Burger. Pramanik [6] studied the heat transfer properties of Casson fluid by utilizing thermal radiation and porous media. Akbar [7] explored the magnetic field's impact over Casson fluid of peristaltic model in the symmetrical tube. Alamri et al. [8] analyzed plane Poiseuille fluid and examined the consequences of second-order slip. Abou-Zeid [9] examined the incompressible non-Newtonian micropolar fluid movement, including heat exchange. Hassan et al. [10] analyzed the movement of water-based nanofluid over wavy surfaces into a permeable medium. Heat exchange features in a

turbulent MHD Casson fluid are explained by Kataria and Patel [11]. Saravana et al. [12] surveyed the effects of aligning the magnetic field over Casson fluid through a stretching layer. Flow and heat exchange applications beyond stretching sheets have a broad variety of technical applications. Fluid flow through the (stretching) surfaces is effective in practicing such as warm evolution, cord drawing, exclusion, and copper twisting. The effects on the Casson fluid by entropy generation and hall impact are explained by Aziz and Afify [13]. Pop and Khan [14] adopted the technique of series solutions on Casson fluid flows over an infinite plate and found their approximate solutions for a dimensionless scheme of ordinary differential equations. Kashif et al. [15] recently put an effort into approximating the results of the nanofluid phenomena with the help of an analytical technique called HAM. However, the same technique has been exercised on the MHD flow analysis by Bayones et al. [16] with mixed convection moving through the plane surface. Seadawy et al. [17] discussed the engrossing non-Newtonian model, advanced for chemical engineering systems as the tangent hyperbolic fluid model, implemented the HAM approach, and discussed the impact of the flow control variables to conceive the complete apprehension of the ongoing pagination and determined that the surface drag factor and convective thermal for the plate are larger in magnitude than for the other geometry. Tripathi and Beg [18, 19] proposed a mathematical simulation of the bioengineering design with the aid of peristaltic structure and nanofluids. In their two studies, Jamshed et al. [20, 21] studied the non-Newtonian nanofluid flow to explore its effects induced by elastic sheets of different nature by finding some approximate solutions and presented some remarkable results. Muhammad et al. [22] present the attributes of a magnetic dipole in a ferro-viscous fluid derived by a plate that is linearly stretched and disclose the prominent effects in regulating the heat transfer effects where the ferro factor is responsible to reduce the axial velocity but raise the temperature distribution. El-dabe et al. [23, 24] considered the Casson MHD flow and examined the various features of substantial parameters. Abou-zeid et al. [25, 26] used the homotopy perturbation method for non-Newtonian MHD nanofluids. 2-D mixed convection with heat transfer effect and concentration flow through a stretched layer was expended by Zeeshan et al. [27]. Pal et al. [28] studied the heat features with the non-Darcy flow in the existence of ohmic distraction, and El-Dabe et al. [29] analyzed the non-Newtonian case and expanded the research of Pal and Mondal [28] for the shrinking surface.

The current research has the novelty that it is an enhanced version in the field of stretching surfaces where the simulations are carried out through the technique of HAM towards the ambient Casson fluid's flow with the involvement of electric and magnetic fields. Also, the effects of viscous dissipation, thermal diffusion, and heat generation are considered or invoked in the energy equation. The convergence regulator through HAM is functional to get the analytic approximation. No one researched it till now. In it, the heat transportation and flow characteristics of Casson fluid are reviewed across a permeable stretching layer with heat production, and their appraisal in the form of series solutions will be discussed. The influence of various physical constraints is examined by utilizing tables and graphs as the heat effects have been investigated with the aid of the Nusselt number in the tabulated form.

2. Problem's Framework

A steady, non-Newtonian, incompressible, two-dimensional, electrically conducting flow through a stretching sheet immersed in a permeable medium is considered. A consistent electric and magnetic field $\vec{E} = (0, 0, -E_0)$ and $\vec{B} = (0, B_0, 0)$ is introduced over the flow region (see Figure 1). Here, $\nabla \times \vec{E} = 0$ and $\nabla \cdot \vec{B} = 0$ are the Maxwell equations, with Ohm's principle $\vec{J} = \sigma(\vec{E} + \vec{v} \times \vec{B})$, where $\vec{J}$ be the fluid current, σ be the magnetic permeability, and $\vec{v}$ be the fluid speed. The momentum and thermal boundary surface equations are revealed in the following along with the influence of the electric and magnetic field. The involvement of chemical reactions and temperature differences in the mass transfer equation is also considered.

The mathematical model with the aid of boundary layer (BL) approximations [28, 30, 31] is obeyed by

$$\frac{\partial \hat{u}}{\partial \hat{x}} + \frac{\partial \hat{v}}{\partial \hat{y}} = 0, \tag{1}$$

$$\hat{u}\frac{\partial \hat{u}}{\partial \hat{x}} + \hat{v}\frac{\partial \hat{u}}{\partial \hat{y}} = \frac{\partial^2 \hat{u}}{\partial \hat{y}^2}\nu\left(1 + \frac{1}{\beta}\right) + \frac{\sigma}{\rho}\left(E_0 B_0 - B_0^2 \hat{u}\right) - \frac{\nu}{k_1}\hat{u}, \tag{2}$$

$$\hat{u}\frac{\partial \hat{T}}{\partial \hat{x}} + \hat{v}\frac{\partial \hat{T}}{\partial \hat{y}} = \frac{k}{\rho C_p}\frac{\partial^2 \hat{T}}{\partial \hat{y}^2} + \frac{\sigma}{\rho C_p}\left(\hat{u}B_0 - E_0\right)^2 - \frac{1}{\rho C_p}\frac{\partial q_r}{\partial \hat{y}} + G\left(\hat{T} - \hat{T}_\infty\right) + \frac{\mu}{\rho C_p}\left(1 + \frac{1}{\beta}\right)\left(\frac{\partial \hat{u}}{\partial \hat{y}}\right)^2, \tag{3}$$

$$\hat{u}\frac{\partial \hat{C}}{\partial \hat{x}} + \hat{v}\frac{\partial \hat{C}}{\partial \hat{y}} = \frac{D_m K_t}{\hat{T}_m}\frac{\partial^2 \hat{T}}{\partial \hat{y}^2} + D_m\frac{\partial^2 \hat{C}}{\partial \hat{y}^2} - A\left(\hat{C} - \hat{C}_\infty\right). \tag{4}$$

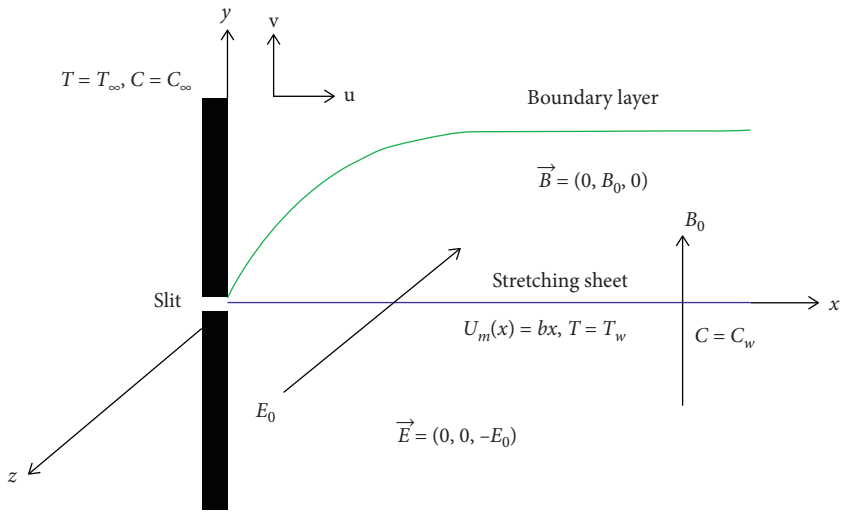

Figure 1: Geometry of the EMHD model.

Here, $\hat{u}$ and $\hat{v}$ are the directional parts of speed relative to $\hat{x}$ and $\hat{y}$ axis, μ be the kinematic thickness, σ be the electrical conduction, ρ be the flow density, k_1 be the permeability of permeable media, k be the thermal conduction, c_p is the specific heat, D_m and K_t are the mass and thermal diffusivity parameters, A indicates the reaction value constant, and $\hat{T}_m$ is the mean flow temperature with end conditions [32]:

$$\begin{cases} \hat{u} = U_m(\hat{x}) = b\hat{x}, \\ \hat{v} = 0, \\ \hat{T} = \hat{T}_w = \hat{T}_\infty + A_0\left(\dfrac{\hat{x}}{l}\right)^2, \\ \hat{C} = \hat{C}_w \text{ when } \hat{y} = 0, \\ \hat{u} = 0, \\ \hat{T} \longrightarrow \hat{T}_\infty, \\ \hat{C} \longrightarrow \hat{C}_\infty \text{ when } \hat{y} \longrightarrow \infty, \end{cases} \tag{5}$$

where $\hat{T}_w$ and $\hat{T}_\infty$ represent the thermal reading of the sheet and ambient surface, respectively, and A_0 is the temperature variation parameter over the stretching layer. The thermal radiation heat flux is

$$q_r = -\left(\frac{3}{4}\right)^{-1}\sigma^* 3k_0^{-1}\left(\hat{T}_y^4\right), \tag{6}$$

where k_0 and σ^* are the parameters of mean absorption and Stefan–Boltzmann law. We considered that the temperature variations in the current flow of the fluid-phase are extremely low; therefore, $\hat{T}^4$ can be displayed as a linear map.

$$\hat{T}^4 = -3\hat{T}_\infty^4 + 4\hat{T}_\infty^3\hat{T}. \tag{7}$$

With the assistance of the following resemblance arrangements,

$$\begin{aligned} \hat{u} &= b\hat{x}\tilde{f}'(\vartheta), \\ \hat{v} &= -\sqrt{b\nu}f(\vartheta), \\ \theta(\vartheta) &= \frac{\hat{T} - \hat{T}_\infty}{\hat{T}_w - \hat{T}_\infty}, \\ \phi(\vartheta) &= \frac{\hat{C} - \hat{C}_\infty}{\hat{C}_w - \hat{C}_\infty}, \\ \vartheta &= \sqrt{\frac{b}{\nu}}\hat{y}, \end{aligned} \tag{8}$$

where f, θ, and ϕ are the dimensional free stream functions and ϑ is the resemblance variable. The above equations (1)–(4) can be converted into the ordinary differential equation

$$\left(1 + \frac{1}{\beta}\right)f''' + ff'' - (f')^2 + \mathrm{Ha}^2(E_1 - f') - K_1 f' = 0, \tag{9}$$

$$\left(\frac{1 + Nr}{\mathrm{Pr}}\right)\theta'' + f\theta' - 2f'\theta + \left(1 + \frac{1}{\beta}\right)E_c f''^2 + E_c\mathrm{Ha}^2(f' - E_1)^2 + G\theta = 0, \tag{10}$$

$$\frac{1}{\mathrm{Sc}}\phi'' + f\phi' - \delta\phi + Sr\theta'' = 0. \tag{11}$$

It is obvious that the above equations are the nonlinear ordinary differential equations for the Casson liquid. If $\beta \longrightarrow \infty$, the fluid becomes ordinary Newtonian, where $Ha^2 = \sigma B_0^2/\rho b$ be the Hartmann number, $K_1 = \nu bx/k$ be the porous measurement, $E_1 = E_0/B_0 bx$ be the electric measurement, $Nr = 16\sigma^* T_\infty^3/3kK$ be the thermal radiation measurement, $\mathrm{Pr} = \rho\nu C_p/K$ be the Prandtl value, $E_c = b^2 l^2/A_0 C_p$ is the Eckert value, $Sc = \nu/D_m$ be the Schmidt number, $\delta = AT_m/D_m k_t$ be the chemical reaction, and $Sr = D_m k_t/\nu T_m (C_w - C_\infty)$ be the Soret number. Furthermore, the appropriate boundary constants are as follows:

$$\begin{cases} \text{As } \vartheta = 0, \\ f(\vartheta) = 0, \\ f'(\vartheta) = 1, \\ \theta(\vartheta) = 1, \\ \phi(\vartheta) = 1, \\ \text{As } \vartheta \longrightarrow \infty, \\ f'(\vartheta) = 0, \\ \theta(\vartheta) = 0, \\ \phi(\vartheta) = 0. \end{cases} \tag{12}$$

The significant factors for the application point of view are involved in equations (9)–(11) to find the rate of change as a frictional factor. Heat transfer and mass transfer in dimensionless shape are functional as

$$\begin{aligned} C_f\sqrt{\mathrm{Re}_x} &= \left(\frac{1+\beta}{\beta}\right) f''(0), \\ N_{u_x}\mathrm{Re}_x^{-1/2} &= -\theta'(0), \\ \mathrm{Sh}_x\mathrm{Re}_x^{-1/2} &= -\phi'(0). \end{aligned} \tag{13}$$

3. Solution by HAM

Equations (9), (10), and (11) are standard nonlinear ordinary differential equations that are dealt with an analytical skill named as homotopic analysis method. Liao was the first [33] to present the homotopy analysis method and the analyzers discovered that it is a dynamic technique to obtain an estimated solution to the problem. The said procedure also avows the choice of a series base solution. The handy guesswork in initial approximation, linear operator, and auxiliary function (for details, see [34, 35]) in the present problem are as follows:

$$f_0(\vartheta) = 1 - \theta_0(\vartheta), \theta_0(\vartheta) = e^{-\vartheta} = \phi_0(\vartheta), \tag{14}$$

where the auxiliary linear operators are

$$\begin{aligned} \frac{\partial^3 f}{\partial\vartheta^3} + \frac{\partial^2 f}{\partial\vartheta^2} &= \overline{\mathscr{L}}_f, \\ \frac{\partial^2\theta}{\partial\vartheta^2} + \frac{\partial\theta}{\partial\vartheta} &= \overline{\mathscr{L}}_\theta, \\ \frac{\partial^2\phi}{\partial\vartheta^2} + \frac{\partial\phi}{\partial\vartheta} &= \overline{\mathscr{L}}_\phi, \end{aligned} \tag{15}$$

having the following properties

$$\begin{aligned} \overline{\mathscr{L}}_f &= C_1 + C_2 e^{-\vartheta}, \\ \overline{\mathscr{L}}_\theta &= C_3 e^{\vartheta} + C_4 e^{-\vartheta}, \\ \overline{\mathscr{L}}_\phi &= C_5 e^{\vartheta} + C_6 e^{-\vartheta}, \end{aligned} \tag{16}$$

with $C_j\,(j = 1 - 6)$ denoting the arbitrary constants. For this, we (for details, see [36, 37]) constructed a zero-order deformation equation with one parameter function of the equation in "s" as

$$\begin{aligned} (1-s)\overline{\mathscr{L}}_f\left[\tilde{f}(\vartheta,s) - f_0(\vartheta)\right] &= s\hbar_f H(\vartheta)\mathscr{N}_f[\tilde{f}(\vartheta,s)], \\ (1-s)\overline{\mathscr{L}}_\theta\left[\tilde{\theta}(\vartheta,s) - \theta_0(\vartheta)\right] &= s\hbar_\theta H(\vartheta)\mathscr{N}_\theta[\tilde{\theta}(\vartheta,s)], \\ (1-s)\overline{\mathscr{L}}_\phi\left[\tilde{\phi}(\vartheta,s) - \phi_0(\vartheta)\right] &= s\hbar_\phi H(\vartheta)\mathscr{N}_\phi[\tilde{\phi}(\vartheta,s)], \\ \tilde{f}(0,s) &= 0, \\ \tilde{f}\prime(0,s) &= 1, \\ \tilde{f}\prime(\infty,s) &= 1, \\ \tilde{\theta}(0,s) &= 1, \\ \tilde{\theta}(\infty,s) &= 0, \\ \tilde{\phi}(0,s) &= 1, \\ \tilde{\phi}(\infty,s) &= 0, \end{aligned} \tag{17}$$

containing nonlinear operators

$$\mathcal{N}_f[\tilde{f}(\vartheta,s)] = \left(1+\frac{1}{\beta}\right)\tilde{f}'''(\vartheta,s) + \tilde{f}(\vartheta,s)\tilde{f}''(\vartheta,s) - \tilde{f}'^2(\vartheta,s) + Ha^2\left(E_1 - \tilde{f}'(\vartheta,s)\right) - K_1\tilde{f}',$$

$$\mathcal{N}_\theta[\tilde{\theta}(\vartheta,s)] = \left(\frac{1+Nr}{\Pr}\right)\tilde{\theta}''(\vartheta,s) + \tilde{f}(\vartheta,s)\tilde{\theta}'(\vartheta,s) - 2\tilde{f}'(\vartheta,s)\tilde{\theta}(\vartheta,s) + \left(1+\frac{1}{\beta}\right)E_c\tilde{f}'^2(\vartheta,s) + E_cHa^2\left(\tilde{f}'(\vartheta,s) - E_1\right)^2 + G\tilde{\theta}(\vartheta,s),$$

$$\mathcal{N}_\phi[\tilde{\phi}(\vartheta,s)] = \left(\frac{1}{Sc}\right)\tilde{\phi}''(\vartheta,s) + \tilde{f}(\vartheta,s)\tilde{\phi}'(\vartheta,s) - \delta\phi(\vartheta,s) + Sr\theta''(\vartheta,s). \tag{18}$$

If $s = 0$ and $s = 1$, then

$$\left\{\tilde{f}(\vartheta,0), \tilde{\theta}(\vartheta,0), \tilde{\phi}(\vartheta,0), \tilde{f}(\vartheta,1), \tilde{\theta}(\vartheta,1), \tilde{\phi}(\vartheta,1)\right\} = \{f_0(\vartheta), \theta_0(\vartheta), \phi_0(\vartheta), f(\eta), \theta(\eta), \phi(\eta)\}, \tag{19}$$

where $s\varepsilon[0,1]$ is an inserting measurement and $\hbar_f, \hbar_\theta$, and $\hbar_\phi$ are nonzero ancillary measurements. $H(\vartheta)$ is an ancillary function, $\overline{\mathscr{L}}_f, \overline{\mathscr{L}}_\theta$, and $\overline{\mathscr{L}}_\phi$ are ancillary linear operators, $f_0(\vartheta), \theta_0(\vartheta)$, and $\phi_0(\vartheta)$ are initial approximations, and $\tilde{f}(\vartheta,s), \tilde{\theta}(\vartheta,s)$, and $\tilde{\phi}(\vartheta,s)$ are anonymous functions (for nitty-gritty, see [36, 37]).

4. Recognition of HAM Solutions

The main feature on which the current analytic solution of an equation depends is the $\hbar$, a convergence regulator. An eye for the convergence criteria is provided or plotted in Figure 2, where the apposite $\hbar$ values are selected from it. For more recognition, Table 1 is presented ahead.

5. Discussion

In this section, the following points are highlighted: (i) influence of the magnetic and electric field, (ii) significance of the features of the permeability of the channel on the flow attributes, (iii) involvement of viscous dissipation in the energy equation, (iv) effect of diffusion species with the addition of the first-order chemical reaction, (v) relative response of the shear thinning fluid model in the feature of uniform porous surface, and (vi) the dimension-free ODEs (9), (10) and, (11) with the respective end-point conditions are solved after utilizing the famous analytic technique HAM. Figure 2 illustrates the curves of $\hbar$-cut for different distributions of the system where the sequence convergence of these series solutions depends strongly on the convergence control parameters h_f, h_θ, and h_ϕ. It is worth explaining that the suitable range for these parameters is $-1.0 \le h_f \le -0.10$, $-1.60 \le h_\theta \le -0.20$, and $-2.80 \le h_\phi \le -0.50$ as observed in Figure 2. Equations (9)–(11) with the constraint of (12) are processed mathematically by the HAM. The different physical parameters such as $\beta = 1$, $K_1 = 0.2$, $Ec = 0.1$, $E_1 = 0.1$, $Ha = 0.1$, $Nr = 0.1$, $G = 0.5$, $\Pr = 3$, $Sc = 1.5$, $\delta = 0.1$, and $Sr = 0.1$ are proposed for the whole impagination unless mentioned in tables. Table 1 presents the features of solutions to convergence criteria via HAM against the suitable values of $\hbar$ as decided by Figure 1. Table 2 provides a distinction between the empirical findings of the current analysis and those reported by Pal and Mondal [28] and El-dabe et al. [23] for the local Nusselt number for the separate values of Pr. It can be observed from the tables that the present findings are in good concordance. It indicates that the skin friction coefficient and local Nusselt number appear as an increasing function of the Prandtl number.

Figures 3 and 4 display the influence of Hartmann value for both velocity as well as temperature distribution, respectively, by fixing the other physical quantities. The profiles explain that, in the absence of an electric field ($E_1 = 0$), raising the Hartmann value clearly reduces the velocity description in the boundary surface. This reduces the boundary surface thickness because of the transverse magnetic field and the temperature field tends to rise (see Figure 4). It is verified from this assumption that, due to the nihility of an electric field, the enforced transversal magnetic field yields a force on the body classified as a Lorentz force that defies the movement of Casson fluid flow. The opposition of that body force over the flow is therefore the source of temperature enhancement. Figures 5 and 6 display that increasing the electric parameter increased the velocity as well as the temperature profile. This examination of the profile declares that the impact of the local electric field parameter E_1 is to carry the streamlines away from the stretching surface. This transformation of streamlines is notably a bit away from the stretching surface. This is because of Lorentz's force, resulting from the electrical field that decreases the frictional opposition, which also helps to reduce the temperature distribution. Figures 7 and 8 arrange the permeability impacts where the velocity description decreases with the rise of the porous permeability measurement, while the opposite pattern is shown for the temperature distribution because of the existence of a permeable media which enhances the opposition to the flow and decreases the fluid speed. As the value of porosity escalates, permeability level decreases, and temperature acts more stable which strengthens the concept of the porous medium. Vivid effects of a Casson factor, which is actually a

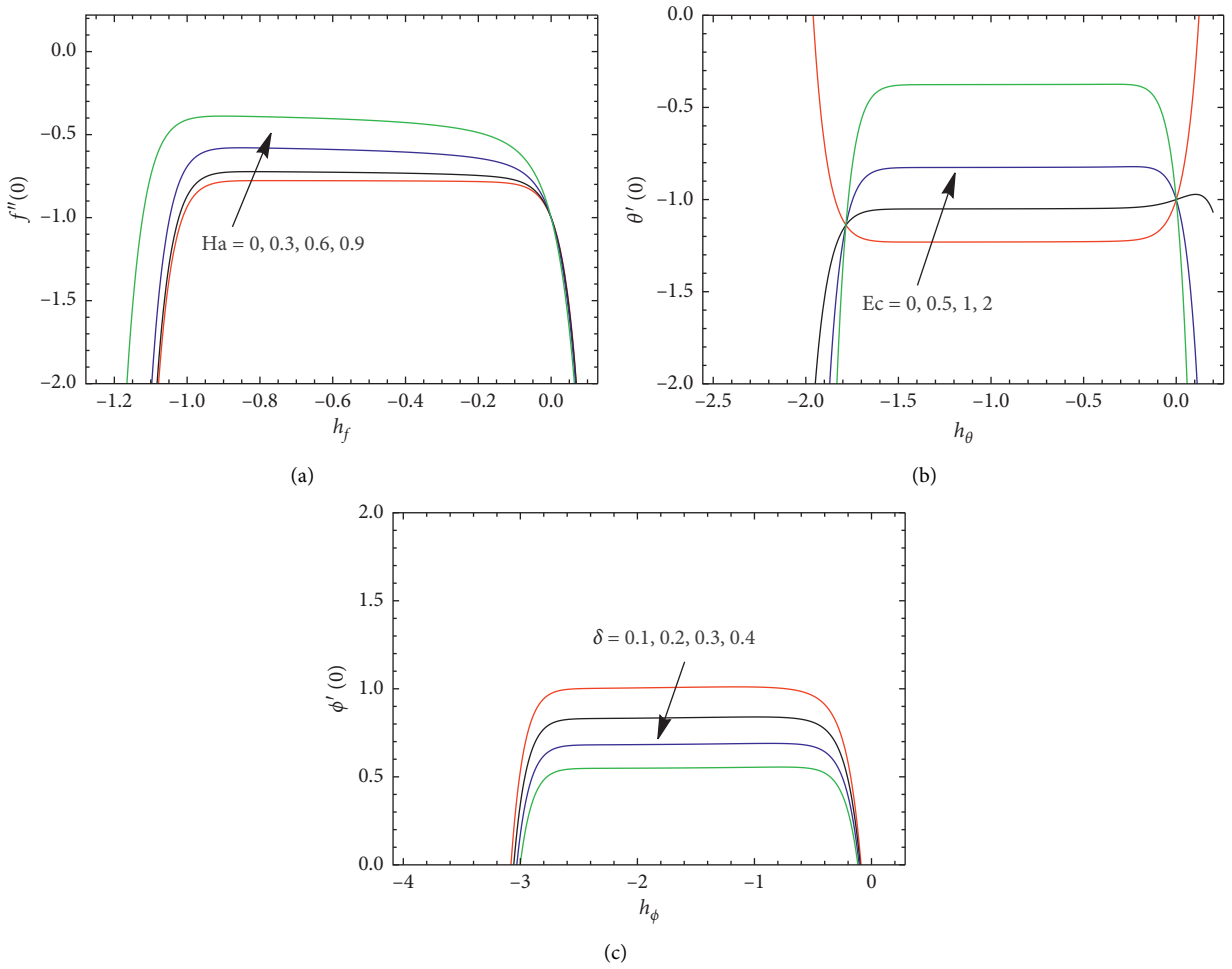

Figure 2: $\hbar$-curves of equations (9), (10), and (11).

Table 1: HAM solution's convergence.

$\beta = 1, K_1 = 0.2, \Pr = 3, E_1 = 0.1, G = 0.5, Ha = 0.1, Ec = 0.1, Nr = 0.1, Sr = 0.1, Sc = 1.5,$ and $\delta = 0.1$.			
Approximation's order	$f''(0)$	$-\theta'(0)$	$-\phi'(0)$
5	−0.7827	1.9855	3.8822
10	−0.77619	2.0032	4.3277
15	−0.7715	2.0079	4.3973
20	−0.7626	2.0114	4.4150
25	−0.7519	2.0231	4.4161
30	−0.7519	2.0231	4.4161
35	−0.7519	2.0231	4.4161
40	−0.7519	2.0231	4.4161

non-Newtonian parameter, can be seen in Figures 9 and 10. An increase in this parameter reduces the viscous characteristic of the fluid; that is why, the larger the Casson factor, the more the fluid is characterized as a Newtonian fluid. All this happens due to the high rate of plasticity in Casson liquid and joule heating within the surface of the plate, so it protects to increase the temperature but decreases the velocity. Figures 11 and 12 represent the influence of the Eckert value and Prandtl value against the temperature description. The Eckert value is actually significant for measuring the dissipation of energy of the flow control as observed in Figure 11. The temperature rises as Ec increases, evident from the assumption that energy is retained in the fluid area due to the viscous heat generation as a result of dissipation due to viscosity. It is observed in Figure 12 that the temperature profile decreases as the Prandtl value increases. This is because thermal BL thickness is shortened by raising the Prandtl value and heat diffuses rapidly from the surface. Also, the heat transfer rates are enhanced at the surfaces of the stretched sheet for more Prandtl number influence. Figure 13 represents that the temperature description increases with the rise in Nr. It exists due to the relative participation of transfer of conduction heat to the thermal radiation relocation. This is because increasing the Nr value implies the increase of radiation in the thermal boundary surface that rises the temperature description. Figure 14 displays that the increasing value of G raises the temperature description due to the increase of heat generation. All this happens in the thermal BL because of the generation of heat which stimulates the temperature to step up. Figures 15 and 16 demonstrate the actions of the concentration for distinct values of Sc and Sr. It has been noticed that the concentration tends to increase with the increase in Sc. This is due to an increase in the Schmidt value, which means a decline in

Table 2: Numerical assessments for $-\theta'(0)$ with several values of Pr against $Ha = 0$.

Pr	$-\theta'(0)$ (present)	$-\theta'(0)$ (Pal and Mondal [28])	$-\theta'(0)$ (El-Dabe et al. [29])
1	1.33329	1.33333	1.19268
2	1.99996	1.99999	1.94141
3	2.50980	2.509715	2.79731
4	2.93876	2.93878	

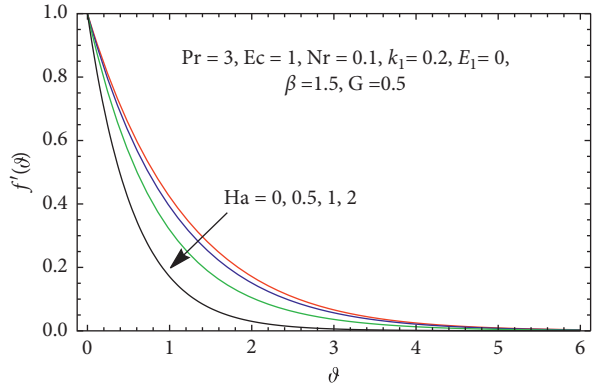

Figure 3: Influence of velocity relative to ϑ for variation of Ha.

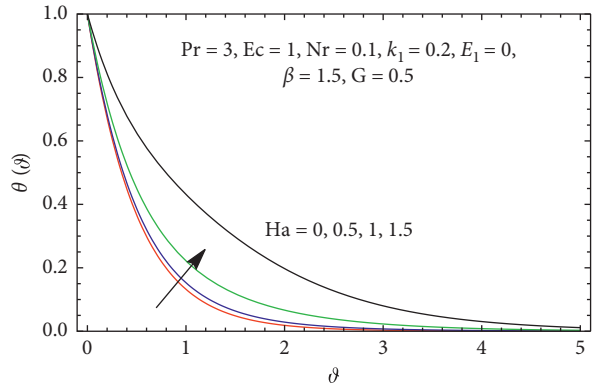

Figure 4: Influence of temperature relative to ϑ for variation of Ha.

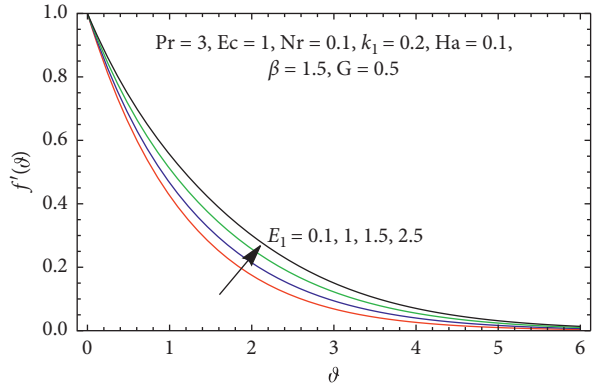

Figure 5: Influence of velocity relative to ϑ for variation of E_1.

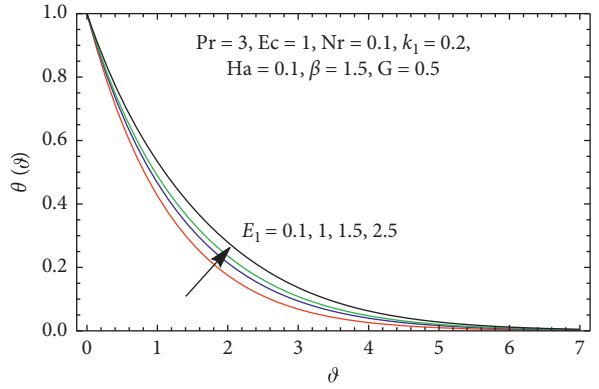

Figure 6: Influence of temperature relative to ϑ for variation of E_1.

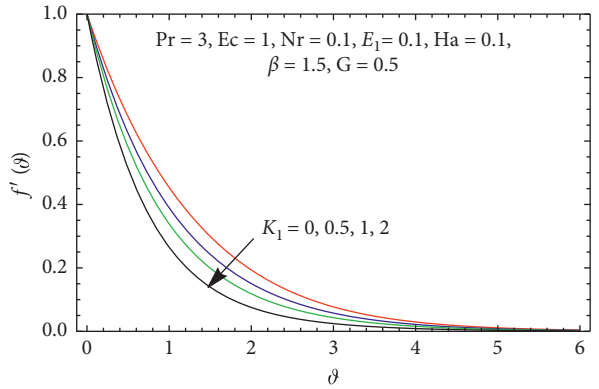

Figure 7: Influence of velocity relative to ϑ for variation of K_1.

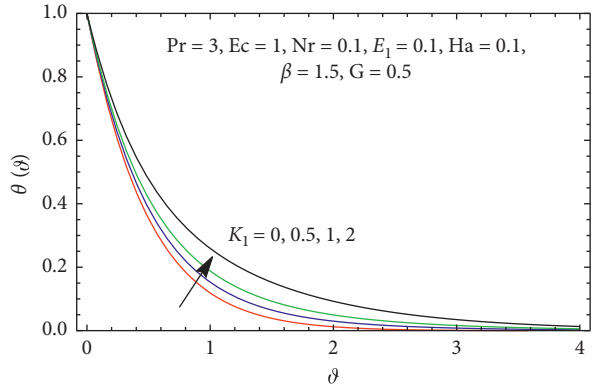

Figure 8: Influence of temperature relative to ϑ for variation of K_1.

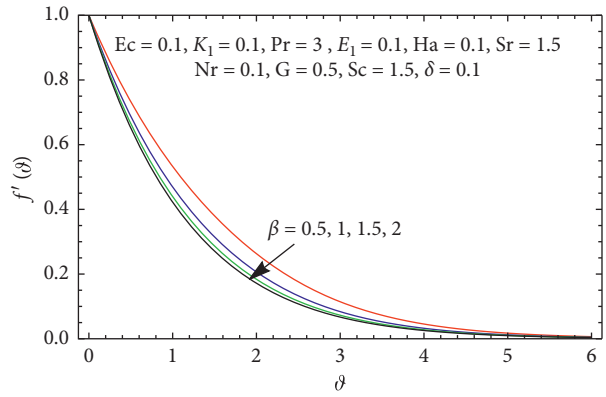

Figure 9: Influence of velocity relative to ϑ for variation of β.

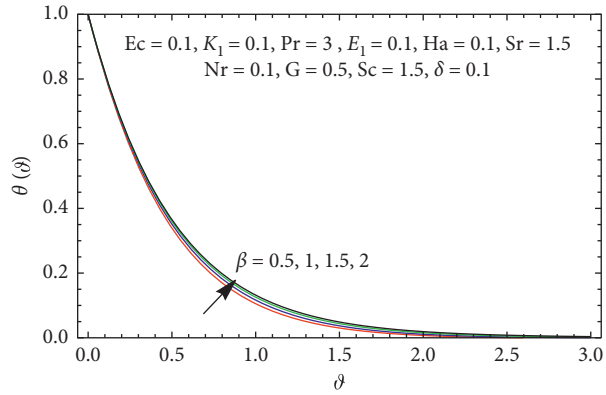

Figure 10: Influence of temperature relative to ϑ for variation of β.

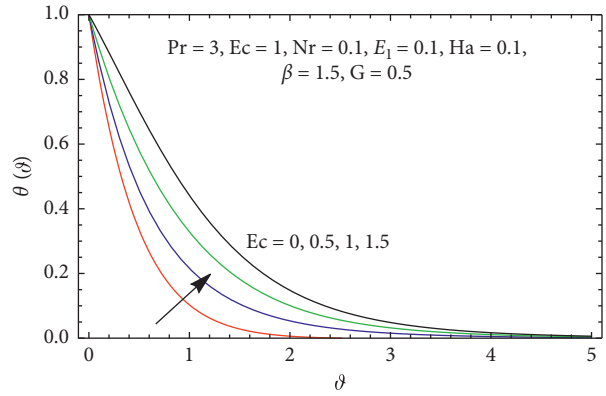

Figure 11: Influence of temperature relative to ϑ for variation of E_c.

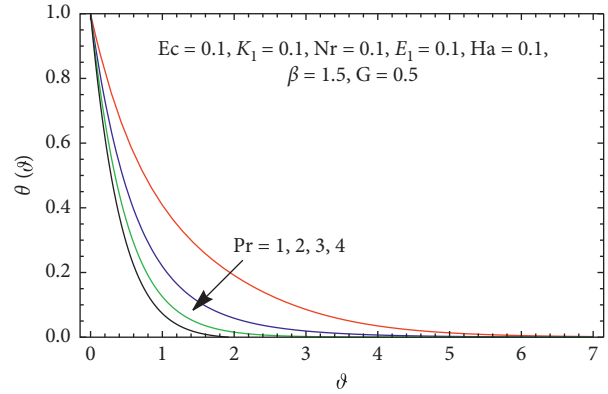

Figure 12: Influence of temperature relative to ϑ for variation of Pr.

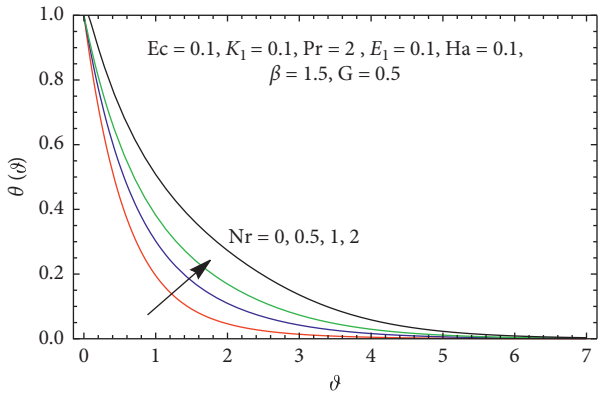

Figure 13: Influence of temperature relative to ϑ for variation of Nr.

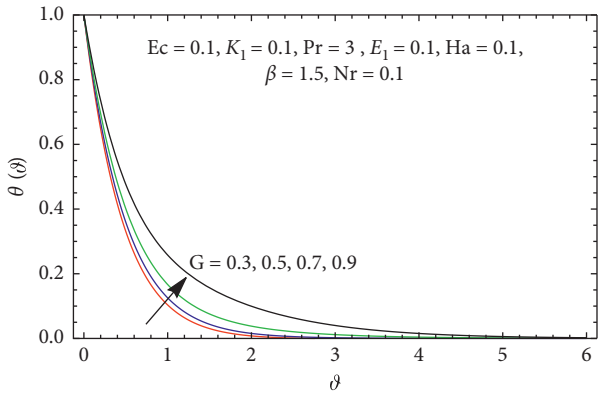

Figure 14: Influence of temperature relative to ϑ for variation of G.

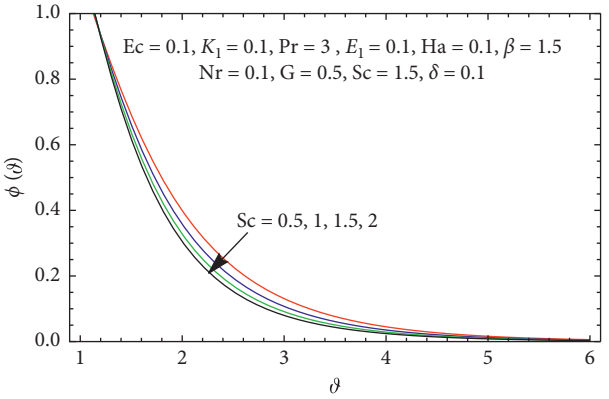

Figure 15: Concentration field relative to ϑ for variation of Sc.

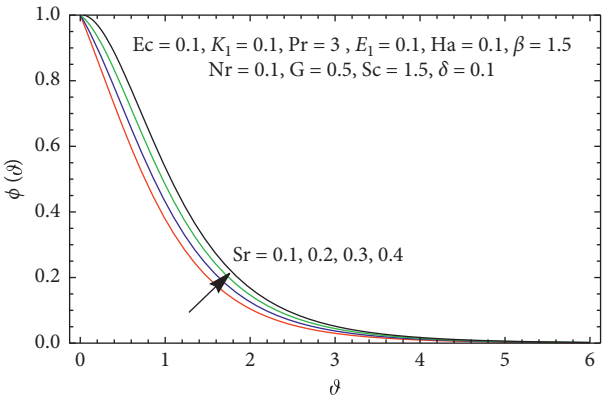

Figure 16: Concentration field relative to ϑ for variation of Sr.

molecular diffusion. Figure 16 displays that the rising values of Sr, and the concentration of Casson liquid is growing in the region of BL as the presence of temperature gradients in species diffusion raises the concentration profile.

6. Conclusions

Analytic simulation has been carried out for the collective study of the BL flow of the EMHD incompressible Casson fluid flow, along with the heat and mass transfer properties over the stretched surface, by taking the influence of Ohmic-viscous dissipation, thermal radiation, chemical reaction, and thermophoresis. From the application point of view, such models are influential in the sector of energy production, which is practicable without higher pumping powers, and are useful in the thermal network for some effective energy gadgets, especially in paper-making, polymer, food processing, panacea's inoculation, and dissipation in arteries, etc. So, the minuscule layout reveals that increasing the value of the magnetic number decreases the temperature profile. Increasing the value of Ha exhibits the reverse flow behavior to the velocity and temperature. Both the profiles are elevated as the electric number increases. Viscous dissipation, porosity, and the Casson parameter (due to its resistive nature) strengthen the temperature profile. But reverse effects against the Prandtl number and rate of heat transfer are an increasing function of Pr. The value of S_c is responsible to weaken the concentration profile but strengthen with S_r. Numerical results were identified with the existing data found in the literature for some confined cases, and good accordance was observed.

7. Future Recommendations

The current impagination will be further probed in the presence of some more conservation laws and then be discussed with the help of some new physical parameters. The said model can also be further probed for fractional order. The considered model can also be solved with the inclusion of entropy generation on different geometries and conditions.

Nomenclature

$\hat{u}, \hat{v}$: Velocity parts along $\hat{x}$, $\hat{y}$ directions $\{ms^{-1}\}$
U_m: Stretched velocity $\{ms^{-1}\}$
B_0: Magnetic field $\{Wbm^{-2}\}$
T: Temperature {K}
T_∞: Ambient temperature {K}
T_w: Surface temperature {K}
C_p: Specific heat $\{Jkg^{-1}K^{-1}\}$
T_m: Mean temperature {K}
C: Fluid's concentration $\{kgm^{-3}\}$
qr: Radiative heat flux $\{Wm^{-2}\}$
σ: Electrical conductivity $(\omega^{-1}m^{-1})$
g: Gravitational acceleration $\{ms^{-2}\}$
D_m: Mass diffusion coefficient $\{m^2s^{-1}\}$
C_w: Concentration of the sheet $\{kgm^{-3}\}$
C_∞: Ambient concentration $\{kgm^{-3}\}$
A: Rate of chemical reaction {–}
Ha: Magnetic parameter {–}
Pr: Prandtl number {–}
E_1: Eckert parameter {–}
Sc: Schmidt number {–}
K_1: permeable parameter {–}
Sr: Soret number {–}
Nr: Thermal radiation parameter {–}

Greek Symbols

β: Casson factor {–}
α: Thermal diffusivity $\{m^2s^{-1}\}$
ρ: Density $\{kgm^{-3}\}$
ν: Kinematic viscosity $\{m^2s^{-1}\}$
f, θ, ϕ: Nondimensional velocity, temperature, and concentration {–}
ϑ: Nondimensional time {–}
Ψ: Stream function
δ: Dimensionless buoyancy parameter {–}.

Data Availability

No data were used to support this work.

Conflicts of Interest

The authors declare that they have no conflicts of interest.

Acknowledgments

The authors acknowledge with thanks Prof. Hammad Alotaibi and Prof. Y. S. Hamed for their useful and valuable suggestions.

References

[1] J. Venkatesan, D. S. Sankar, K. Hemalatha, and Y. Yatim, "Mathematical analysis of Casson fluid model for blood rheology in stenosed narrow arteries," *Journal of Applied Mathematics*, vol. 2013, pp. 1–11, Article ID 583809, 2013.

[2] N. Thamaraikannan, S. Karthikeyan, D. K. Chaudhary, and S. Kayikci, "Analytical investigation of magnetohydrodynamic non-Newtonian type Casson nanofluid flow past a porous channel with periodic body acceleration," *Complexity*, vol. 2021, Article ID 7792422, 17 pages, 2021.

[3] H. Shahzad, X. Wang, I. Sarris, K. Iqbal, M. B. Hafeez, and M. Krawczuk, "Study of non-Newtonian biomagnetic blood flow in a stenosed bifurcated artery having elastic walls," *Scientific Reports*, vol. 11, no. 1, 2021.

[4] N. Thamaraikannan, S. Karthikeyan, and D. K. Chaudhary, "Significance of MHD radiative non-Newtonian nanofluid flow towards a porous channel: a framework of the Casson Fluid Model," *Journal of Mathematics*, vol. 2021, Article ID 9912239, 15 pages, 2021.

[5] A. Ali, A. Fatima, Z. Bukhari, H. Farooq, and Z. Abbas, "Non-Newtonian Casson pulsatile fluid flow influenced by Lorentz force in a porous channel with multiple constrictions," *A numerical study, Korea-Aust. Rheol. J.*no. 33, pp. 79–90, 2021.

[6] S. Pramanik, "Casson fluid flow and heat transfer past an exponentially porous stretching surface in presence of thermal radiation," *Ain Shams Engineering Journal*, vol. 5, no. 1, pp. 205–212, 2014.

[7] N. Sher Akbar, "Influence of magnetic field on peristaltic flow of a Casson fluid in an asymmetric channel: application in crude oil refinement," *Journal of Magnetism and Magnetic Materials*, vol. 378, pp. 463–468, 2015.

[8] S. Z. Alamri, R. Ellahi, N. Shehzad, and A. Zeeshan, "Convective radiative plane Poiseuille flow of nanofluid through porous medium with slip: an application of Stefan blowing," *Journal of Molecular Liquids*, vol. 273, pp. 292–304, 2019.

[9] M. Abou-zeid, "Effects of thermal-diffusion and viscous dissipation on peristaltic flow of micropolar non-Newtonian nanofluid: application of homotopy perturbation method," *Results in Physics*, vol. 6, pp. 481–495, 2016.

[10] M. Hassan, M. Marin, A. Alsharif, and R. Ellahi, "Convective heat transfer flow of nanofluid in a porous medium over wavy surface," *Physics Letters A*, vol. 382, no. 38, pp. 2749–2753, 2018.

[11] H. R. Kataria and H. R. Patel, "Heat and mass transfer in magnetohydrodynamic (MHD) Casson fluid flow past over an oscillating vertical plate embedded in porous medium with ramped wall temperature," *Prop. Pow. Res*, vol. 7, no. 9, pp. 257–267, 2018.

[12] R. Saravana, M. Sailaja, and R. Hemadri Reddy, "Effect of aligned magnetic field on Casson fluid flow over a stretched surface of non-uniform thickness," *Nonlinear Engineering*, vol. 8, no. 1, pp. 283–292, 2019.

[13] M. Abd El-Aziz and A. A. Afify, "MHD Casson fluid flow over a stretching sheet with entropy generation analysis and hall influence," *Entropy*, vol. 21, no. 6, p. 592, 2019.

[14] L. Pop and W. Khan, "Boundary-layer flow of a nanofluid past a stretching sheet," *International Journal of Heat and Mass Transfer*, vol. 53, pp. 2477–2483, 2010.

[15] K. A. Khan, N. Raza, and M. Inc, "Insights of numerical simulations of MHD squeezing nanofluid flow through a channel with permeable walls, Pro," *Power Research*, vol. 1, pp. 146–154, 2021.

[16] F. S. Bayones, K. S. Nisar, K. A. Khan et al., "Magneto-hydrodynamics (MHD) flow analysis with mixed convection moves through a stretching surface," *AIP Advances*, vol. 11, no. 4, Article ID 045001, 2021.

[17] A. Seadawy, N. Raza, O. H. Khalil, K. A. Khan, and M. Usman, "Computational approach and flow analysis of chemically reactive tangent hyperbolic nanofluid over a cone and plate," *Waves in Random and Complex Media*, pp. 1–15, 2021.

[18] O. A. Bég and D. Tripathi, "Mathematica simulation of peristaltic pumping with double-diffusive convection in nanofluids: a bio-nano-engineering model," *Proceedings of the Institution of Mechanical Engineers - Part N: Journal of Nanoengineering and Nanosystems*, vol. 225, no. 3, pp. 99–114, 2012.

[19] D. Tripathi and O. A. Bég, "A study on peristaltic flow of nanofluids: application in drug delivery systems," *International Journal of Heat and Mass Transfer*, vol. 70, pp. 61–70, 2014.

[20] W. Jamshed, "Numerical investigation of MHD impact on Maxwell nanofluid," *International Communications in Heat and Mass Transfer*, vol. 120, Article ID 104973, 2021.

[21] T. Mukhtar, W. Jamshed, A. Aziz, and W. Al-Kouz, "Computational investigation of heat transfer in a flow subjected to magnetohydrodynamic of Maxwell nanofluid over a stretched flat sheet with thermal radiation," *Numerical Methods for Partial Differential Equations*, 2020.

[22] N. Muhammad, S. Nadeem, and M. T. Mustafa, "Impact of magnetic dipole on a thermally stratified ferrofluid past a stretchable surface," *J. Process Mech. Eng.*, 2018.

[23] N. T. M. El-dabe, M. Y. Abou-zeid, and Y. M. Younis, "Magnetohydrodynamic peristaltic flow of Jeffry nanofluid with heat transfer through a porous medium in a vertical tube," *Applied Mathematics & Information Sciences*, vol. 11, no. 4, pp. 1097–1103, 2017.

[24] N. T. M. El-Dabe, A. A. Shaaban, M. Y. Abou-Zeid, and H. A. Ali, "Magnetohydrodynamic non-Newtonian nanofluid flow over a stretching sheet through a non-Darcy porous medium with radiation and chemical reaction," *Journal of Computational and Theoretical Nanoscience*, vol. 12, no. 12, pp. 5363–5371, 2015.

[25] M. Y. Abou-zeid and M. A. A. Mohamed, "Homotopy perturbation method for creeping flow of non-Newtonian power-law nanofluid in a nonuniform inclined channel with peristalsis," *Zeitschrift für Naturforschung A*, vol. 72, no. 10, pp. 899–907, 2017.

[26] M. Y. Abou-zeid, "Homotopy perturbation method for MHD non-Newtonian nanofluid flow through a porus medium in eccentric annuli in peristalsis," *Thermal Science*, vol. 5, no. 21, pp. 2069–2080, 2017.

[27] A. Zeeshan, A. Majeed, R. Ellahi, and M. Z. Zia, "Mixed convection flow and heat transfer in ferromagnetic fluid over a stretching sheet with partial slip effects," *Thermal Science*, vol. 22, no. 6, pp. 2515–2526, 2018.

[28] D. Pal and H. Mondal, "Hydromagnetic non-Darcy flow and heat transfer over a stretching sheet in the presence of thermal radiation and Ohmic dissipation," *Communications in Nonlinear Science and Numerical Simulation*, vol. 15, no. 5, pp. 1197–1209, 2010.

[29] N. T. El-Dabe, M. Y. Abou-Zeid, O. H. El-Kalaawy, S. M. Moawad, and O. S. Ahmed, "Electromagnetic steady motion of Casson fluid with heat and mass transfer through porous medium past a shrinking surface," *Thermal Science*, vol. 25, p. 416, 2019.

[30] S. Shateyi and S. S. Motsa, "Hydromagnetic non-Darcy flow, heat and mass transfer over a stretching sheet in the presence of thermal radiation and Ohmic dissipation," *Canadian Journal of Chemical Engineering*, vol. 89, no. 6, pp. 1388–1400, 2011.

[31] P. O. Olanrewaju, "Effects of internal heat generation on hydromagnetic non-Darcy flow and heat transfer over a stretching sheet in the presence of thermal," *Radiation and Ohmic Dissipation*, vol. 16, pp. 37–45, 2012.

[32] J. Bear, *Dynamics of Fluids in Porous Media*, Dover, Mineola, NY., 1972.

[33] S. Liao, "On the homotopy analysis method for nonlinear problems," *Applied Mathematics and Computation*, vol. 147, no. 2, pp. 499–513, 2004.

[34] K. A. Khan, A. R. Butt, and N. Raza, "Influence of porous medium on magneto hydrodynamics boundary layer flow through elastic sheet with heat and mass transfer," *Journal of Nanofluids*, vol. 8, no. 4, pp. 725–735, 2019.

[35] K. A. Khan, A. R. Butt, N. Raza, and K. Maqbool, "Unsteady magneto-hydrodynamics flow between two orthogonal moving porous plates," *Eur. Phys. J. Plus*, vol. 1, p. 134, 2019.

[36] K. A. Khan, A. R. Butt, and N. Raza, "Effects of heat and mass transfer on unsteady boundary layer flow of a chemical reacting Casson fluid," *Results in Physics*, vol. 8, pp. 610–620, 2018.

[37] K. A. Khan, A. R. Seadawy, and A. Jhangeer, "Numerical appraisal under the influence of the time dependent Maxwell fluid flow over a stretching sheet," *Mathematical Methods in the Applied Sciences*, vol. 44, 2020.